SENSEI: Characterization of Single-Electron Events Using a Skipper Charge-Coupled Device

Liron Barak,[1] Itay M. Bloch,[1] Ana Botti,[2,3] Mariano Cababie,[2,3,*] Gustavo Cancelo,[3] Luke Chaplinsky,[4,5] Fernando Chierchie,[3] Michael Crisler,[3] Alex Drlica-Wagner,[3,6,7] Rouven Essig,[4] Juan Estrada,[3] Erez Etzion,[1] Guillermo Fernandez Moroni,[3] Daniel Gift,[4,5] Stephen E. Holland,[8] Sravan Munagavalasa,[4,5] Aviv Orly,[1] Dario Rodrigues,[2,3] Aman Singal,[5] Miguel Sofo Haro,[3,9] Leandro Stefanazzi,[3] Javier Tiffenberg,[3] Sho Uemura,[1] Tomer Volansky,[1] and Tien-Tien Yu[10]
(SENSEI Collaboration)

[1] *School of Physics and Astronomy, Tel-Aviv University, Tel-Aviv 69978, Israel*
[2] *Department of Physics, FCEN, University of Buenos Aires and IFIBA, CONICET, Buenos Aires, Argentina*
[3] *Fermi National Accelerator Laboratory, PO Box 500, Batavia, Illinois 60510, USA*
[4] *C.N. Yang Institute for Theoretical Physics, Stony Brook University, Stony Brook, New York 11794, USA*
[5] *Department of Physics and Astronomy, Stony Brook University, Stony Brook, New York 11794, USA*
[6] *Kavli Institute for Cosmological Physics, University of Chicago, Chicago, Illinois 60637, USA*
[7] *Department of Astronomy and Astrophysics, University of Chicago, Chicago, Illinois 60637, USA*
[8] *Lawrence Berkeley National Laboratory, One Cyclotron Road, Berkeley, California 94720, USA*
[9] *Centro Atómico Bariloche, CNEA/CONICET/IB, Bariloche, Argentina*
[10] *Department of Physics and Institute for Fundamental Science, University of Oregon, Eugene, Oregon 97403, USA*

(Received 2 July 2021; revised 22 September 2021; accepted 23 December 2021; published 19 January 2022)

We use a science-grade skipper charge-coupled device (skipper CCD) operating in a low-radiation background environment to develop a semiempirical model that characterizes the origin of single-electron events in CCDs. We identify, separate, and quantify three independent contributions to the single-electron events, which were previously bundled together and classified as "dark counts": dark current, amplifier light, and spurious charge. We measure a dark current, which depends on exposure, of $(5.89 \pm 0.77) \times 10^{-4}$ e^-/pix/day, and an unprecedentedly low spurious charge contribution of $(1.52 \pm 0.07) \times 10^{-4}$ e^-/pix, which is exposure independent. In addition, we provide a technique to study events produced by light emitted from the amplifier, which allows the detector's operation to be optimized to minimize this effect to a level below the dark-current contribution. Our accurate characterization of the single-electron events allows one to greatly extend the sensitivity of experiments searching for dark matter or coherent neutrino scattering. Moreover, an accurate understanding of the origin of single-electron events is critical to further progress in ongoing research and development efforts of skipper and conventional CCDs.

DOI: 10.1103/PhysRevApplied.17.014022

I. INTRODUCTION

Charge-coupled devices (CCDs) have been widely used photon detectors for scientific purposes since their invention in 1969 [1,2]. More recently, they have also been adopted as particle detectors in rare-event searches for coherent neutrino scattering [3] and dark matter particles [4,5]. The development of the skipper CCD [6], with its deep subelectron readout noise and resulting ability to detect events producing only a single photon or a single electron, has revolutionized the search for coherent neutrino scattering and dark matter particles, since these produce events typically containing only one or a few ionized electrons [7,8]. The first science results from data collected with a single skipper CCD have already been presented in Refs. [9–11], and the construction of large-mass detectors for both neutrino and dark matter particles searches is underway or planned [11–14].

The data from Refs. [9–11] contain a large number of single-electron events (SEEs). A detailed understanding of the nature and origin of these SEEs in silicon crystals, and in (skipper) CCDs in particular, is crucial both for maximizing the sensitivity to coherent neutrino scattering and to dark matter and for assessing the discovery potential of these experiments.

*mcababie@df.uba.ar

We present in this paper a set of techniques to identify and characterize the nature and origin of SEEs, utilizing a science-grade skipper CCD. We employ a skipper CCD from the first batch of sensors fabricated using ultrahigh-resistivity silicon ($R > 18$ kΩ). We also propose a semiempirical model that describes the observed SEEs. The methodology described here provides a set of techniques that we expect can be implemented with any skipper CCDs. Furthermore, it enables current and planned experiments utilizing skipper CCDs, such as CONNIE, SENSEI, DAMIC-M, and Oscura, to mitigate these background events and greatly enhance their sensitivity to, and discovery potential of, coherent neutrino scattering and sub-GeV dark matter.

II. TECHNICAL DESCRIPTION

We provide here a brief description of the skipper CCD and the data taking.

A. The skipper CCD

The measurements presented in this work were performed using a science-grade skipper CCD from the SENSEI experiment [11]. The sensors were designed by the Lawrence Berkeley National Laboratory (LBNL), and fabricated at Teledyne/DALSA using high-resistivity (>18 kΩ-cm) silicon wafers with a thickness of 675 μm. The packaging and testing of the sensors was done at the SiDet facility at the Fermi National Accelerator Laboratory (FNAL) using the package design described in Ref. [11]. The sensor was installed in a vacuum vessel that was placed in a low-radiation environment at the MINOS underground facility at FNAL. The shielding surrounding the skipper CCD can be divided into an "internal" and an "external" shield, corresponding to whether it was installed inside or outside of the vacuum vessel that houses the skipper CCD. An external shield was added in the midst of the data-taking process. For details on both types of shielding, see Ref. [11].

The skipper CCD used for this work has four identical readout stages, one in each corner. The usual mode of operation is to read out one quarter (a quadrant) of the skipper CCD through the corresponding sensor, simultaneously and independently of the readout of the other quadrants. However, there are no physical barriers between the quadrants and it is possible to read the entire skipper CCD though any one of the readout stages if desired. The active area is a standard LBNL three-phase CCD with a buried p-channel fabricated on a high-resistivity n-type bulk [15]. Each column of pixels is separated by "channel stops," highly doped regions that prevent the spread of the charges from one column into another. The fabrication process for this detector is optimized for dark matter searches, and no polishing of the backside (usually referred to as "thinning") is done to preserve as much target mass as possible. The silicon bulk is fully depleted at approximately 40 V but is operated at a 70 V substrate voltage to reduce the diffusion of charge to neighboring pixels in the bulk.

TABLE I. Main characteristics of the skipper CCD used in this work.

	Value	Units
CCD dimensions	6144×886	pixels
Pixel size	15×15	μm^2
Thickness	675	μm
Total mass	1.926	g
CCD temperature	135	K
Number of amplifiers	4 (2 used)	
Readout time (1 sample)	42.825	μs
Readout noise (1 sample)	2.5	e^- rms/pix
Readout noise (n samples)	$2.5/\sqrt{n}$	e^- rms/pix

The detector is operated at low temperature (135 K) to reduce the probability of surface and bulk electrons being promoted into the conduction band due to thermal agitation [2]. At this temperature, the fraction of thermally induced events, which we refer to as "intrinsic dark current," is subdominant compared to other sources of charge [11]. Operating the sensor at even lower temperatures has the undesirable effect of increasing the charge transfer inefficiency. As there is an unusual excess of SEEs in the third quadrant and a high charge transfer inefficiency in the fourth quadrant, the data collected by these two quadrants are not used in the final analysis. A brief summary of the skipper CCD's characteristics is given in Table I.

As shown in Fig. 1, each quadrant of the CCD can be divided into four regions: active area, transfer gate, serial register, and readout stage. The active area of each quadrant is an array of 3072×443 pixels where the charges are collected during the exposure of the CCD sensor. A schematic depiction of the readout stage is provided in Fig. 2.

B. Data-taking cycle

The standard data-taking cycle of a CCD consists of three phases.

(a) *Cleaning.* During this phase, the substrate bias of the CCD is set at 0 V [15], whereas voltages from the vertical clocks on the surface of the CCD are set at 9 V in order to invert the surface with electrons from the channel stops [16], filling the surface traps and thereby reducing intrinsic dark current and "resetting" the CCD. At the end of this procedure, the substrate voltage is set back to the depletion voltage and the surface clocks are set to their previous configuration. The entire CCD is then read out in order to remove all of the accumulated charge so that one can start the next phase with a "clean" CCD.

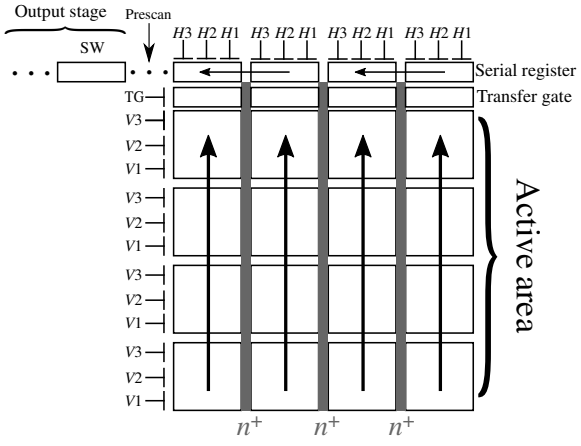

FIG. 1. Schematic illustration of a 4×4 pixels quadrant of a CCD. The arrows show the direction in which collected charges are transferred during readout. A detailed schematic of the readout stage is provided in Fig. 2. Here $H1$, $H2$, and $H3$ are the last horizontal clocks in the serial register before the summing well (SW). Highly doped n-type "channel stops" are shaded gray.

(b) *Exposure.* During this phase all voltages are kept fixed. Any ionizing interaction that occurs within the active area of the detector therefore leaves electrons trapped inside the pixels, which are later read during the readout phase. The bias voltage V_{DD} for the output transistor $M1$ is set to 0 during this phase and turned on during the other phases.

(c) *Readout.* The collected charges are transferred vertically row by row into the serial register through the transfer gate. Once the charges reach the serial register, they are transported horizontally, one pixel at a time, to the readout stage (Fig. 1). At the readout stage, the charges collected in each pixel are converted into a voltage signal that is finally measured by the readout electronics (Fig. 2).

III. SEMIEMPIRICAL MODEL FOR THE ORIGIN OF THE SINGLE-ELECTRON EVENTS

The SEEs per pixel have two main contributions that scale with time: events produced during exposure (μ_{exp}) and events produced during readout (μ_{ro}). The rates of these contributions are expected to be different as the amount of light produced by the readout stage depends on the base current of the output transistor, which varies during readout and is turned off during the exposure phase under normal operating conditions. We identify also a time-independent contribution, which we define as spurious charge (μ_{SC}). Spurious charge is generated when the surface voltages of the pixels in the active area, transfer gate, and serial register change in order to transfer charge from one pixel to the other. Such events are produced during the cleaning and readout phases and will be discussed later. Since they depend solely on the number of times a pixel is clocked (i.e., the number of times a pixel transfers charges to its neighbor), they are modeled as an additional exposure-independent term.

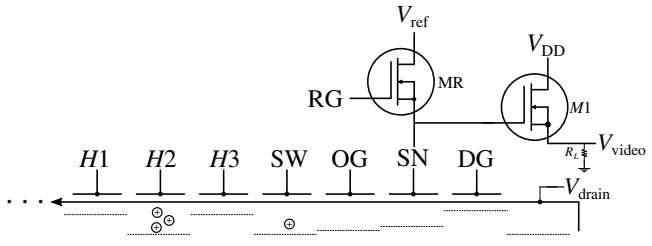

FIG. 2. Schematic illustration of a skipper-CCD readout stage [6]. Here $H1$, $H2$, and $H3$ are the last horizontal clocks in the serial register before the SW. OG, corresponds to the output gate, SN, to the sense node, DG the dump gate and RG the reset gate.

Following these definitions, the total number (μ) of SEEs per pixel generated during a data-taking cycle can be written as

$$\begin{aligned}\mu(t_{exp}, t_{ro}) &= \mu_{exp}(t_{exp}) + \mu_{ro}(t_{ro}) + \mu_{SC} \\ &= \lambda_{exp} t_{exp} + \lambda_{ro} t_{ro} + \mu_{SC}, \end{aligned} \tag{1}$$

where in the second line we have assumed that both μ_{exp} and μ_{ro} scale linearly with time. The parameters λ_{exp} and λ_{ro} are the SEE rates during the exposure and readout phases, respectively, in units of events per pixel per day, while the times t_{exp} and t_{ro} are expressed in days.

There are three contributions to the SEEs: dark current, amplifier light, and spurious charge. In the following subsection we discuss each of these contributions in detail. In that discussion, these contributions will be classified based on the following primary characteristics: spatial distribution (localized or uniform) and time dependence. Throughout our analysis we use the event-selection criteria discussed in Ref. [11] and summarized in Table I of that paper, with the exception of the edge mask and the halo mask (cut numbers 6 and 9 of Table I of Ref. [11]), which we set to 40 pixels (instead of 60) to increase the statistics for this work.

A. Dark current

Although the CCD is inside a sealed vacuum vessel, SEEs can be generated in the CCD during both exposure and readout, even in the absence of any external source (except unavoidable environmental radiation interactions) and is unrelated to charges being shifted from pixel to pixel. We refer to SEEs generated in this way as dark current (DC) and differentiate between two distinct contributions, intrinsic and extrinsic, depending on whether the current is generated by the CCD itself (intrinsic) or through an interaction with its environment (extrinsic). DC contributes during both the exposure and readout phases of data taking. The number of events coming from DC scales

linearly with time during the exposure phase and hence λ_{DC}, the rate of SEEs generated from DC, will be one of the components of λ_{exp}. During the readout phase, the exposure of the pixels is nonuniform as the last pixel read has an additional exposure time of t_{ro} when compared to the pixel that is read first. Overall, the average contribution of the DC during the readout phase is given by $\lambda_{DC}/2$.

1. Intrinsic dark current

Intrinsic dark current (usually referred plainly as dark current in the literature) is the most well-studied current contribution for SEEs [2,17]. This source generates, via thermal fluctuations across the silicon bandgap, single electron-hole pairs. The holes, which we collect using a *p*-buried channel, are trapped in the potential wells within the pixels. Since this thermal agitation is a random process independent of time and space, the number of holes collected from the thermal agitation in a pixel for a given period of time is a random variable that follows a Poisson distribution. The expected value is the intrinsic DC rate multiplied by the exposure time of the pixel. We can further differentiate between two types of intrinsic DC that appear in a buried-channel CCD: bulk and surface intrinsic DC. The latter component can be greatly reduced, at least temporarily, with an inversion of the surface in the cleaning phase [16]. This empties the traps that mediate the generation of surface DC. The traps begin to fill again during the subsequent exposure phase, but this recovery is inhibited at low temperature. Estimates from the model developed in Ref. [18] show that less than 0.1% of the surface intrinsic DC is recovered at the operating temperature of 135 K after 24 h (much longer than any measurement carried out during this work). Therefore, we find that the bulk component dominates the intrinsic DC.

2. Extrinsic dark current

In Ref. [11], we reported a SEE rate of $(1.594 \pm 0.160) \times 10^{-4}$ e^-/pix/day, which, despite being the lowest value ever reported in a CCD, is at least one order of magnitude above the theoretically expected intrinsic DC rate at 135 K. This discrepancy is explained by additional environmentally induced contributions to the observed SEEs, distributed approximately uniformly across the CCD (after applying the event-selection criteria and with the given statistical uncertainties) and, as the intrinsic DC, increasing linearly with the exposure time. In this sense it is, in principle, indistinguishable from the intrinsic DC. This extrinsic contribution was identified in Ref. [11] and is directly related to the environmental radiation. A detailed discussion of the physical processes that likely explain these SEEs is discussed in Ref. [19].

B. SEEs produced by amplifier light

As the number of SEEs per pixel decreases with lower temperature and background radiation as well as improved detector performance, additional low-energy signals appear that are not contained in the definition of DC. This collaboration recently reported an excess of SEEs near the readout stage [10], which we refer to as amplifier-light events. This effect was previously investigated by many authors [20–24] and is due to infrared photons emitted by the $M1$ transistor of the readout stage (see Fig. 2). Because the photons have a finite range in silicon and are emitted continuously, charge generated by this effect is spatially localized in the region near the readout stage and increases linearly with time. We express the corresponding rate as λ_{AL} (in units of events per pixel per day). As this contribution is localized, λ_{AL} depends not only on the distance from the readout stage but on which zone of the CCD is under study. For the sake of simplicity, we average λ_{AL} over the whole CCD and do not study the spatial dependence.

Since V_{DD} is set to 0 during exposure, SEEs due to amplifier light are only produced in readout and cleaning phases. Note that if V_{DD} is kept on during the exposure phase, an additional non-negligible amplifier-light contribution must be taken into account. That contribution may be different, since the voltage in the floating gate (which is also the gate of the $M1$ transistor; see Fig. 2) is constant during exposure but changes rapidly during readout. Moreover, as the active area is being read and pixels are being transported to the sense node, the spatial dependence of the amplifier light during the readout and exposure phases is different.

C. Spurious charge

The last SEE contribution to take into consideration is the spurious charge (SC), which is generated when the voltages in the active area or serial register are clocked [2,25,26]. As noted earlier, SCs are generated during both cleaning and readout phases and depend solely on the number of times a pixel is clocked. Therefore, the SC is a spatially uniform, time-independent, intrinsic contribution to the SEE.

D. Empirical model

Given the three contributions discussed in the previous sections, we can express both λ_{exp} and λ_{ro} as

$$\lambda_{exp} = \lambda_{DC}, \tag{2}$$

$$\lambda_{ro} = \frac{\lambda_{DC}}{2} + \lambda_{AL}, \tag{3}$$

TABLE II. Summary of charge contributions and their properties, following Eq. (4). The units for λ_{DC} and λ_{AL} are e^-/pix/day, while μ_{SC} is in e^-/pix. At 135 K and after an inversion of the CCD surface, the intrinsic DC is dominated by the bulk intrinsic DC, which has a clear linear time dependence; we can ignore the surface intrinsic DC that has a nonlinear time dependence.

Contribution (e^-/pix)		Time dependence			Spatial distribution
		Linear		Independent	
		Exposure	Readout		
Dark current	Intrinsic	$\lambda_{DC} t_{exp}$	$(\lambda_{DC}/2) t_{ro}$	...	Uniform
	Extrinsic				Uniform
Amplifier-light current		...	$\lambda_{AL} t_{ro}$	...	Localized
Spurious charge		...	...	μ_{SC}	Uniform

and rewrite Eq. (1) to obtain our full empirical model:

$$\mu_{(t_{exp},t_{ro})} = \lambda_{DC} t_{exp} + \left(\frac{\lambda_{DC}}{2} + \lambda_{AL}\right) t_{ro} + \mu_{SC}. \quad (4)$$

A summary of the charge contributions that enter Eq. (4) can be found in Table II. In the next section, we use this model to characterize SEEs in a SENSEI skipper CCD.

IV. SINGLE-ELECTRON EVENT TRANSFER CURVES

Using the model in Eq. (4), we propose a set of methods to measure λ_{DC}, λ_{AL}, and μ_{SC}. These techniques provide the "transfer curves" for SEEs as a function of both exposure and readout times. We use two techniques to measure all of the parameters in Eq. (4).

I. *Determination of* λ_{DC}. We record several images with a range of different exposure times and a fixed readout time. For each image (with a given exposure time), we measure the amount of SEEs per pixel. We then plot the SEEs per pixel as a function of the exposure time and perform a linear fit. The slope of this linear function corresponds to λ_{DC} as shown in Eq. (5), and the y intercept is the SEE rate from the readout (μ_{ro} for a fixed readout time t_{ro}) plus the SC (μ_{SC}):

$$\mu(t_{exp}) = \lambda_{DC} t_{exp} + (\mu_{ro} + \mu_{SC}). \quad (5)$$

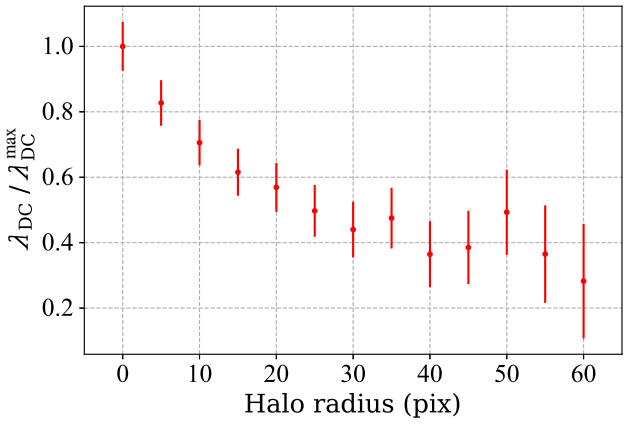

FIG. 3. The normalized dark current rate, λ_{DC}, as a function of the halo radius mask. As can be seen, λ_{DC} monotonically decreases until a halo radius of roughly 30 pixels. Dataset *A* is used for this figure.

II. *Determination of* λ_{AL} *and* μ_{SC}. Using the measured value for λ_{DC} obtained by the previous procedure, λ_{AL} and μ_{SC} can be measured by taking multiple images with different readout times and zero exposure time. To avoid changing the geometry of the active area (and hence the value of λ_{AL}), t_{ro} is varied by changing the number of samples that are taken per pixel (see the Appendix for a study of SC generation in the readout stage). For each image (with a given readout time), we measure the amount of SEEs per pixel. We then plot the SEEs as a function of t_{ro} and perform a linear fit. The slope of this linear function is $(\lambda_{DC}/2) + \lambda_{AL}$ as shown in Eq. (6), while the y intercept is μ_{SC}:

$$\mu(t_{ro}) = \left(\frac{\lambda_{DC}}{2} + \lambda_{AL}\right) t_{ro} + \mu_{SC}. \quad (6)$$

V. RESULTS AND DISCUSSION

We study four datasets (see Table III).

Dataset A. To determine λ_{DC}, eight images are taken, each with a different exposure time t_{exp} but the same readout time t_{ro}.

Dataset B. To study the amplifier-light contribution, nine datasets are analyzed, each consisting of six zero-exposure images; each set consists of a different V_{DD} voltage value applied in the $M1$ transistor (see Fig. 2), scanning from -17 to -25 V in 1 V steps.

Datasets C *and* D. To measure μ_{SC} and λ_{AL}, seven datasets are used, each consisting of two zero-exposure images and a different readout time t_{ro}. We use two different experimental configurations: for the first (dataset *C*), we set V_{DD} at -22 V while avoiding the use of an external shield (same as dataset *A*). For the second (dataset *D*), we set the V_{DD} at -21 V and add an additional external shield (see the discussion in Sec. II).

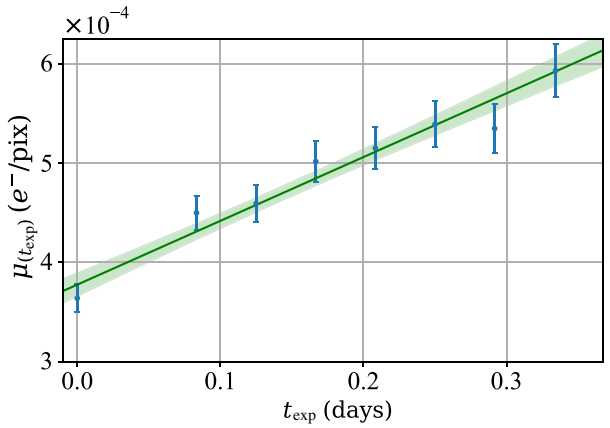

FIG. 4. Determination of λ_{DC}. SEE rate as a function of the exposure time t_{exp} (blue circles). The linear regression of these measurements together with a 1σ C.L. band is shown in green. The slope is found to be $(5.89 \pm 0.77) \times 10^{-4}$ e^-/pix/day and the y intercept $(3.69 \pm 0.13) \times 10^{-4}$ e^-/pix. Dataset A is used for this figure.

As mentioned before, the same event-selection criteria shown in Table I of Ref. [11] are used, except that the edge and halo masks are set to 40 pixels (instead of 60 pixels) in order to increase statistics (see Fig. 3).

A. Dark current

Using dataset A, we extract the number of SEEs per pixel for each image and perform a linear regression using Eq. (5), taking the exposure time of each image t_{exp} as the independent variable. As shown in Fig. 4, we obtain a DC rate of $\lambda_{DC} = (5.89 \pm 0.77) \times 10^{-4}$ e^-/pix/day. This value is compatible with the $(5.312^{+1.490}_{-1.277}) \times 10^{-4}$ e^-/pix/day reported in Ref. [11] for the configuration without the external shield.

Our measurement identifies a non-negligible value of the time-independent term $(\mu_{ro} + \mu_{SC})$ [see Eq. (5)]. This contribution dominates the number of SEEs for exposures shorter than 15 h. To trace its origin and to disentangle the contributions from μ_{ro} and μ_{SC}, we perform a dedicated study to understand the SEEs produced by luminescence of the output transistor. Light generated in the readout stage can reach the pixels in the serial register and active area of the CCD during readout and produce SEEs that are independent of the exposure time. The next subsection discusses this characterization effort and how it leads to the optimization of the operation parameters.

B. Optimization of the operation parameters

To characterize the amplifier-light contribution, we study the impact on the amplifier-light events from varying the voltages in the readout stage. We focus on the voltage applied to the V_{DD} gate, which controls the drain voltage of the output transistor $M1$ (see Fig. 2), as previous works [21,22] have shown that an increase in the current between the drain and source leads to an increase in light emission; this phenomenon is explained in the literature as bremsstrahlung radiation produced by hot electrons. These are electrons that, because of very localized high electric fields in the $M1$ transistor, make a transition from the valence to the conduction band, enabling photon emission as explained in Ref. [21].

To measure the amplifier-light contribution, we take zero-exposure images for nine different V_{DD} values (dataset B) to check if it impacts the number of SEEs collected. As discussed at the end of the previous subsection, light emitted by the output transistor can produce SEEs during readout with a number that is independent of the exposure time. By taking zero-exposure images we are able to measure $\mu_{(t_{ro})}$ as a function of V_{DD}. Following Eq. (6), and using the values of λ_{DC} and μ_{SC} from Table IV (for the corresponding V_{DD} and external shield presence), we can estimate a value of λ_{AL} for each V_{DD} voltage. The origins of both λ_{DC} and μ_{SC} are explained in the next subsection.

In Fig. 5 we show, for each V_{DD} voltage in dataset B, the SEE rate of the total events collected $(\mu_{(t_{ro})})$ in black and the AL contribution (μ_{AL}) extracted for each of those voltages in blue, estimated as $\lambda_{AL} t_{ro}$. It can be seen that the AL contribution to the overall SEE rate drastically decreases between -24 and -21 V, while both signals

TABLE III. Description of each dataset in the section analysis specifying the skipper samples (number of samples measured for a given pixel), V_{DD} voltage (voltage applied to the $M1$ transistor drain channel as shown in Fig. 2), external lead shield presence, and both the exposure and readout times. These last two, as also the number of skipper samples, vary from image to image in the same dataset as explained in the text.

	Dataset			
	A	*B*	*C*	*D*
Skipper samples	250	250	200–950	200–950
V_{DD} voltage ($-V$)	22	17–25	22	21
External shield	No	Yes	No	Yes
Exposure time (hs)	0–8	0	0	0
Readout time (h:m:s)	4:57:00	0:55:43	Variable	Variable

TABLE IV. Summary of charge contributions and results for $V_{DD} = 21$ and -22 V. The units for λ_{DC} and λ_{AL} are 10^{-4} e^-/pix/day, while μ_{SC} is in 10^{-4} e^-/pix. Both λ_{AL} and μ_{SC} from the first two rows are extracted from Fig. 6, whereas λ_{DC} in the first row is obtained from Ref. [11] and in the second row from dataset *A*, as explained above. Additionally, the third row shows λ_{AL} extracted from Fig. 5, as explained in the text.

V_{DD}	External shield	λ_{DC}	λ_{AL}	μ_{SC}
-21	Yes	(1.59 ± 0.16)	(0.36 ± 0.18)	(1.52 ± 0.07)
-22	No	(5.89 ± 0.77)	(19.91 ± 1.26)	(1.59 ± 0.12)
-22	Yes	...	(23.89 ± 3.99)	...

reach a plateau above -21 V. This plateau, that corresponds to μ_{SC} (black dashed line) for $\mu_{(t_{ro})}$, is due to a decrease of light emission in $M1$ as it is driven from its saturation region (below -21 V) to its linear region. At the same time, a reduction of the V_{DD} value produces an increase in the electronic readout noise, which reduces the signal-to-noise ratio. Our technique allows one to optimize the operating conditions depending on the application.

It is not clear due to uncertainties if λ_{AL} is zero for values above -21 V. To quantify this in a more precise way, we take two sets of images with different t_{ro} (datasets *C* and *D*). These data also allow us to measure the amount of SC events under these conditions.

C. Spurious charge and amplifier-light contribution

To measure the parameters in Eq. (6), the following procedure is applied on both datasets *C* and *D*: the amount of SEEs per pixel is extracted for each group of images with equal t_{ro} and a linear regression is performed. Figure 6 illustrates this result for dataset *D*. Following Eq. (6), the slope of the regression is the sum of $\lambda_{DC}/2$ and λ_{AL}, and the y intercept is the amount of SC (μ_{SC}). For $V_{DD} = -22$ V, and using the value for λ_{DC} obtained from dataset *A*, λ_{AL} is determined to be $(19.91 \pm 1.26) \times 10^{-4}$ e^-/pix/day. For $V_{DD} = -21$ V (the configuration used in Ref. [11]), we use the reported λ_{DC} from that work, $(1.59 \pm 0.16) \times 10^{-4}$ e^-/pix/day, as a reference value for λ_{DC}.

The first two rows of Table IV summarize the results after combining Eq. (6) and the values obtained from the linear regression for $V_{DD} = -21$ V and $V_{DD} = -22$ V, as explained in the previous paragraph. Additionally, an estimation of λ_{AL} extracted from Fig. 5 is included in the third row in order to compare results for λ_{AL} with and without an external shield. As shown, the optimization of the V_{DD} voltage from -22 to -21 V reduces the number of amplifier-light events by 2 orders of magnitude. Additionally, the y-intercept values (μ_{SC}) for both datasets *C* and *D* (first two rows of Table IV) are compatible and do not

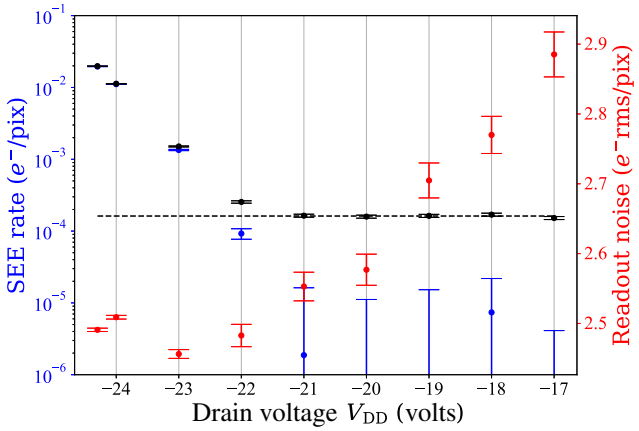

FIG. 5. SEEs per pixel (left axis) and single-sample readout noise (red, right axis) as a function of the drain voltage of the $M1$ transistor (V_{DD}). In black, we show the SEEs per pixel collected for each voltage ($\mu_{(t_{ro})}$) and in blue the AL contribution (μ_{AL}), estimated from Eq. (6). The black dashed line shows the estimation for μ_{SC}. Images are taken from dataset *B*.

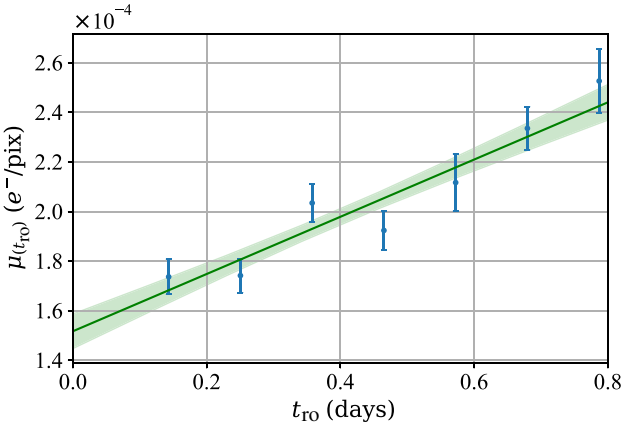

FIG. 6. Determination of λ_{AL} and μ_{SC}. Extracted SEE rate versus readout time t_{ro} (blue dots) for images in dataset *D*. We plot in green the performed linear regression together with a 1σ CL band in light green. The extracted value for the slope of the regression is $(1.15 \pm 0.16) \times 10^{-4}$ e^-/pix/day and the y intercept $(1.52 \pm 0.07) \times 10^{-4}$ e^-/pix.

depend on V_{DD}, or on the additional shielding, as expected. We are currently working on the development of methods to reduce the SC through the shaping of the clock profiles.

VI. CONCLUSIONS

In this work, we provide an empirical model together with the tools to identify and measure the main contributions to SEEs in skipper-CCD sensors. Using these techniques, we are able to identify, disentangle, and quantify individual contributions to the SEE rate previously grouped under the label "dark counts." Our results determine three types of rates: the dark current, a current of single events produced by amplifier light, and the spurious charge. In addition, by studying the dependence of the amplifier light on the drain voltage of the output transistor, we reduced this contribution by 2 orders of magnitude. The empirical modeling and techniques presented in this work provide a tool to optimize the operating conditions and push forward the capability of dark matter experiments based on the skipper-CCD technology.

ACKNOWLEDGMENTS

We are grateful for the support of the Heising-Simons Foundation under Grant No. 79921. This work is supported by Fermilab under DOE Grant No. DE-AC02-07CH11359. The CCD development work is supported in part by the Director, Office of Science, of the DOE under Grant No. DE-AC02-05CH11231. R.E. acknowledges support from DOE Grant No. DE-SC0009854, Simons Investigator in Physics Award 4623940, and US-Israel Binational Science Foundation Grant No. 2016153. The work of D.G. is supported in part by DOE Grant No. DE-SC0009854 and BSF Grant No. 2016153. T.V. is supported by the Israel Science Foundation-NSFC (Grant No. 2522/17), by the Binational Science Foundation (Grant No. 2016153), and by the European Research Council (ERC) under the EU Horizon 2020 Programme (ERC-CoG-2015 - Proposal n. 682676 LDMThExp). The work of S.U. is supported in part by the Zuckerman STEM Leadership Program. I.B. is grateful for the support of the Alexander Zaks Scholarship, the Buchmann Scholarship, and the Azrieli Foundation. This manuscript has been coauthored by employees of Fermi Research Alliance, LLC under Contract No. DE-AC02-07CH11359 with the U.S. Department of Energy, Office of Science, Office of High Energy Physics. The U.S. Government retains, and the publisher, by accepting the article for publication, acknowledges that the U.S. Government retains a nonexclusive, paid-up, irrevocable, worldwide license to publish or reproduce the published form of this manuscript or allows others to do so for U.S. Government purposes.

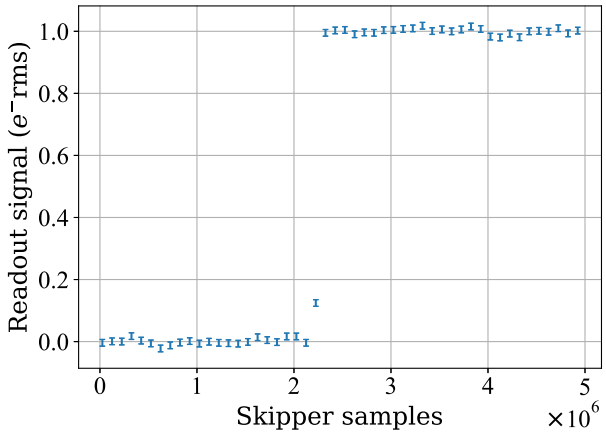

FIG. 7. Readout signal for a given pixel versus the number of skipper samples. A "jump" in the signal can be seen between 2 and 3 million pixels, corresponding to charge generation.

APPENDIX: SPURIOUS CHARGE IN THE READOUT STAGE

In order to measure the generation of SC in the readout stage, we carried out a dedicated study using a skipper CCD installed at SNOLAB in Sudbury, Canada. This CCD is identical to that used for the rest of the work (it is part of the same fabrication batch), and the operating conditions (vacuum pressure and CCD temperature) used during the data-taking process were also similar. While the shielding was slightly different, this will not be relevant for our study of SC generation in the readout stage, as will be clear below. Furthermore, the value of VDD during readout was set at -21 V.

The main goal of the study was to measure if SC generation in the readout stage is a major contribution to the overall SC. In order to do that, 1146 empty pixels with 5 000 000 skipper samples each were read clocking only the readout stage. This amounts to 5.73×10^9 samples.

For additional information on the skipper-CCD operation, we refer the reader to Refs. [2,6].

To identify the generation of charges during this process, all pixels were analyzed to look for "jumps" in the signal, i.e., charge generation. This was done by dividing the 5 000 000 samples of each pixel into 50 groups of 100 000. A "jump" was identified if the mean of a group was away from the next one by at least 5 standard deviations of the former group but less than $100e^-$, an energy threshold from which it was considered that a high-energy event had interacted with the readout stage during the skipper process. An example of a jump is shown in Fig. 7.

Within the 5.73×10^9 samples dataset, 51 "jumps" were found, giving us an event rate of $(8.9 \pm 1.3) \times 10^{-9}$ events/sample if we attribute all these events to SC generated in the readout stage.

For the data collected in the main part of the paper, the number of samples were always less than 1200

samples. This would produce a SC rate of $(1.1 \pm 0.2) \times 10^{-5}$ events/pix or e^-/pix, which is negligible when compared to overall SC contribution. For a regular DM science run, for which approximately 300–400 skipper samples are taken [11], a SC rate of approximately 3×10^{-6} e^-/pix is expected from the readout stage.

It is yet to be understood how many of these events come from luminescence from the readout stage itself and how many from actual SC.

[1] George E. Smith, Nobel lecture: The invention and early history of the CCD, Rev. Mod. Phys. **82**, 2307 (2010).

[2] James Janesick, *Scientific Charge-Couple Devices* (Bellingham, WA, SPIE Optical Engineering Press, 2001), xvi, 906 p. SPIE Press monograph, PM 83. ISBN 0819436984 **83** (2001).

[3] Alexis Aguilar-Arevalo *et al.* (CONNIE Collaboration), Exploring low-energy neutrino physics with the coherent neutrino nucleus interaction experiment, Phys. Rev. D **100**, 092005 (2019).

[4] J. Barreto *et al.* (DAMIC Collaboration), Direct search for low mass dark matter particles with CCDs, Phys. Lett. B **711**, 264 (2012).

[5] A. Aguilar-Arevalo *et al.* (DAMIC Collaboration), Constraints on Light Dark Matter Particles Interacting with Electrons From Damic at Snolab, Phys. Rev. Lett. **123**, 181802 (2019).

[6] Javier Tiffenberg, Miguel Sofo-Haro, Alex Drlica-Wagner, Rouven Essig, Yann Guardincerri, Steve Holland, Tomer Volansky, and Tien-Tien Yu, Single-Electron and Single-Photon Sensitivity with a Silicon Skipper CCD, Phys. Rev. Lett. **119**, 131802 (2017).

[7] Daniel Z. Freedman, Coherent neutrino nucleus scattering as a probe of the weak neutral current, Phys. Rev. D **9**, 1389 (1974).

[8] Rouven Essig, Jeremy Mardon, and Tomer Volansky, Direct detection of sub-GeV dark matter, Phys. Rev. D **85**, 076007 (2012).

[9] Michael Crisler, Rouven Essig, Juan Estrada, Guillermo Fernandez, Javier Tiffenberg, Miguel Sofo Haro, Tomer Volansky, and Tien-Tien Yu, SENSEI: First Direct-Detection Constraints on Sub-GeV Dark Matter from a Surface Run, Phys. Rev. Lett. **121**, 061803 (2018).

[10] Orr Abramoff, Liron Barak, Itay M. Bloch, Luke Chaplinsky, Michael Crisler, Dawa Alex Drlica-Wagner, Rouven Essig, Juan Estrada, Erez Etzion, Guillermo Fernandez, Daniel Gift, Miguel Sofo-Haro, Joseph Taenzer, Javier Tiffenberg, Tomer Volansky, Tien-Tien Yu (SENSEI Collaboration), SENSEI: Direct-Detection Constraints on Sub-GeV Dark Matter From a Shallow Underground Run Using a Prototype Skipper CCD, Phys. Rev. Lett. **122**, 161801 (2019).

[11] Liron Barak *et al.* (SENSEI Collaboration), SENSEI: Direct-Detection Results on Sub-GeV Dark Matter From a New Skipper CCD, Phys. Rev. Lett. **125**, 171802 (2020).

[12] Guillermo Fernandez-Moroni, Pedro A. N. Machado, Ivan Martinez-Soler, Yuber F. Perez-Gonzalez, Dario Rodrigues, and Salvador Rosauro-Alcaraz, The physics potential of a reactor neutrino experiment with skipper CCDS: Measuring the weak mixing angle, ArXiv:2009.10741 (2020).

[13] N. Castelló-Mor, DAMIC-M experiment: Thick, silicon CCDs to search for light dark matter, Nucl. Instrum. Methods Phys. Res., Sect. A **958**, 162933 (2020). Proceedings of the Vienna Conference on Instrumentation 2019.

[14] OSCURA dark matter experiment based on skipper-CCD technology, https://astro.fnal.gov/science/dark-matter/oscura/.

[15] Stephen E. Holland, William F. Kolbe, and Christopher J. Bebek, Device design for a 12.3-megapixel, fully depleted, back-illuminated, high-voltage compatible charge-coupled device, IEEE Trans. Electron. Devices **56**, 2612 (2009).

[16] Stephen E. Holland, Donald E. Groom, Nick P. Palaio, Richard J. Stover, and Mingzhi Wei, Fully depleted, back-illuminated charge-coupled devices fabricated on high-resistivity silicon, IEEE Trans. Electron. Devices **50**, 225 (2003).

[17] Ralf Widenhorn, Morley M. Blouke, Alexander Weber, Armin Rest, and Erik Bodegom, in *Sensors and Camera Systems for Scientific, Industrial, and Digital Photography Applications III*, Vol. 4669, edited by Nitin Sampat, John Canosa, Morley M. Blouke, John Canosa, and Nitin Sampat, International Society for Optics and Photonics (SPIE, San José, CA, USA, 2002), p. 193.

[18] Barry E. Burke and Stephanie A. Gajar, Dynamic suppression of interface-state dark current in buried-channel CCDs, IEEE Trans. Electron. Devices **38**, 285 (1991).

[19] Peizhi Du, Daniel Egana-Ugrinovic, Rouven Essig, and Mukul Sholapurkar, Sources of low-energy events in low-threshold dark matter detectors, ArXiv:2011.13939 (2020).

[20] Dirk Jan Bartelink, J. L. Moll, and N. I. Meyer, Hot-electron emission from shallow *p*-*n* junctions is silicon, Phys. Rev. **130**, 972 (1963).

[21] Akira Toriumi, Makoto Yoshimi, Masao Iwase, Yutaka Akiyama, and Kenji Taniguchi, A study of photon emission from *n*-channel Mosfet's, IEEE Trans. Electron. Devices **34**, 1501 (1987).

[22] Massimo Lanzoni, Enrico Sangiorgi, Claudio Fiegna, Manfredo Manfredi, and Bruno Ricco, Extended (1.1–2.9 eV) hot-carrier-induced photon emission in *n*-channel Si MOSFETs, IEEE Electron Device Lett. **12**, 341 (1991).

[23] Jeff Bude, Nobuyuki Sano, and Akira Yoshii, Hot-carrier luminescence in Si, Phys. Rev. B **45**, 5848 (1992).

[24] J. C. Tsang and J. A. Kash, Picosecond hot electron light emission from submicron complementary metal–oxide–semiconductor circuits, Appl. Phys. Lett. **70**, 889 (1997).

[25] Miguel Sofo Haro, Gustavo Cancelo, Guillermo Fernandez Moroni, Xavier Bertou, Javier Tiffenberg, Eduardo Paolini, and Juan Estrada, in *2016 Argentine Conference of Micro-Nanoelectronics, Technology and Applications (CAMTA)* (IEEE, Neuquen, Argentina, 2016), p. 11.

[26] Miguel Haro, Guillermo Moroni, Javier Tiffenberg, Gustavo Cancelo, Juan Estrada, Xavier Bertou, and Eduardo Paolini, Taking the CCDs to the ultimate performance for low threshold experiments, Tech. Rep. (Fermi National Accelerator Lab. (FNAL), Batavia, IL, USA, 2016).